

ZIF-8 Derived Graphene-Based Nitrogen-Doped Porous Carbon Sheets as Highly Efficient and Durable Oxygen Reduction Electrocatalysts**

Hai-xia Zhong, Jun Wang, Yu-wei Zhang, Wei-lin Xu, Wei Xing, Dan Xu, Yue-fei Zhang, and Xin-bo Zhang*

Abstract: Nitrogen-doped carbon (NC) materials have been proposed as next-generation oxygen reduction reaction (ORR) catalysts to significantly improve scalability and reduce costs, but these alternatives usually exhibit low activity and/or gradual deactivation during use. Here, we develop new 2D sandwich-like zeolitic imidazolate framework (ZIF) derived graphene-based nitrogen-doped porous carbon sheets (GNPCSs) obtained by *in situ* growing ZIF on graphene oxide (GO). Compared to commercial Pt/C catalyst, the GNPCSs show comparable onset potential, higher current density, and especially an excellent tolerance to methanol and superior durability in the ORR. Those properties might be attributed to a synergistic effect between NC and graphene with regard to structure and composition. Furthermore, higher open-circuit voltage and power density are obtained in direct methanol fuel cells.

The oxygen reduction reaction (ORR) always occurs as the bottleneck of fuel cells and metal–air batteries due to its sluggish kinetics.^[1–3] Nowadays, nitrogen-doped porous carbon (NPC) materials have been emerging as very promising metal-free ORR catalysts, wherein the introduced nitrogen atoms could induce the uneven charge distribution of

carbon atoms and thus improve the O₂ adsorption and reduction.^[4] To this end, various nitrogen-containing precursors and templates have been employed to construct porous NCs.^[5–11] However, the obtained catalysts show insufficient activity and poor stability due to poor electrical conductivity of NCs and their corrosion during ORR.^[12,13] Porous metal–organic frameworks (MOFs) are a new family of crystalline porous materials.^[14] Among them, the zeolitic imidazolate framework (ZIF-8) with a high carbon content and large surface area is a good candidate to synthesize porous carbon directly upon carbonization.^[14] In particular, the nitrogen-containing methylimidazole ligand can act as the precursor for NPC. However, as the size of a MOF crystal is limited and, even worse, the breakdown inside the MOF crystal could not be avoided during carbonization, the direct carbonization of a dissociative MOF crystal cannot achieve the consecutive electronic conductivity required for ORR. In response, anchoring ZIF-8 on GO and then carbonizing to GNPCSs could be a good alternative.^[13a,15]

To exert the synergistic effect between ZIF-8 derived NPC and GO-derived graphene, homogenous and complete coating of ZIF-8 on GO is of paramount importance to ensure the efficient generation of abundant NPC on graphene and especially their close contact to achieve a consecutive conductive network, which is crucial for ORR electrocatalysts in terms of N-doped active sites and electron/mass transport. However, although MOF/GO composites have been synthesized and successfully used in fields of, e.g., gas/organic molecules sorption/separation, electrode material, and luminescence, they are not well qualified carbonization precursors for efficient ORR electrocatalysts, because the nitrogen-free and oxygen-rich ligand and hard-to-evaporate metal composing the MOFs and especially their irregular and aggregated morphology would result in inefficient N doping and poor electronic conductivity and porous structure.^[16] To the best of our knowledge, there are only a few reports on successful control of homogenous and complete coating of dispersive GO with a MOF,^[16g–i,17c] which might be due to the fact that pristine GO easily aggregates and lacks adequate functional groups, which are required for oriented MOF growth on its surface. Therefore, the development of a facile and effective strategy to construct dispersive GO/MOF nanosheets with a uniform and complete MOF coating toward efficient NPC precursors is highly desirable but still very challenging.

Herein, to ensure homogenous growth of ZIF-8 on GO, the insufficient functional groups on the GO surface, which are unsuitable as coordination sites for ZIF-8 nucleation, are

[*] H.-x. Zhong,^[†] J. Wang,^[†] D. Xu, Prof. Dr. X.-b. Zhang
State Key Laboratory of Rare Earth Resource Utilization
Changchun Institute of Applied Chemistry
Chinese Academy of Sciences, Changchun, 130022 (P. R. China)
E-mail: xbzhang@ciac.ac.cn
Homepage: energy.ciac.jl.cn

H.-x. Zhong,^[†] J. Wang,^[†]
University of Chinese Academy of Sciences
Beijing, 100049 (China)

Y.-w. Zhang, W.-l. Xu, Prof. W. Xing
State Key Laboratory of Electroanalytical Chemistry
Changchun Institute of Applied Chemistry
Chinese Academy of Science, Changchun, 130022 (China)
Prof. Dr. Y.-f. Zhang
Beijing University of Technology, Beijing, 100124 (P. R. China)

[†] These authors contributed equally to this work.

[**] We appreciate the constructive comments and insightful suggestions of the referees. This work was supported by the 100 Talents Programme of the Chinese Academy of Sciences, the National Program on Key Basic Research Project of China (973 Program, grant no. 2014CB932300 and 2012CB215500), and the National Natural Science Foundation of China (grant no. 21422108, 51472232, and 21271168).



Supporting information for this article is available on the WWW under <http://dx.doi.org/10.1002/anie.201408990>.

enriched with the amide carbonyl groups of poly(vinyl pyrrolidone) (PVP). Those might then coordinate with Zn ions (see below) and thus facilitate the uniform nucleation of ZIF-8 on the surface of GO. Interestingly, the dispersive 2D sandwich-like ZIF-8/GO composite was successfully synthesized. After carbonization, the GNPCs exhibit a high activity, good tolerance to methanol, and superior durability in the ORR compared to a commercial Pt/C catalyst. Furthermore, higher open-circuit voltage and power density were obtained in direct methanol fuel cells.

The fabrication of GNPCs is shown in Scheme S1. The evolution of morphology, structure, and composition during the synthesis of GNPCs-800 were investigated by scanning electron microscopy (SEM), transmission electron microscopy (TEM), and X-ray diffraction (XRD). As shown in Figure 1 a, GO/ZIF-8 inherits the sheet morphology of GO

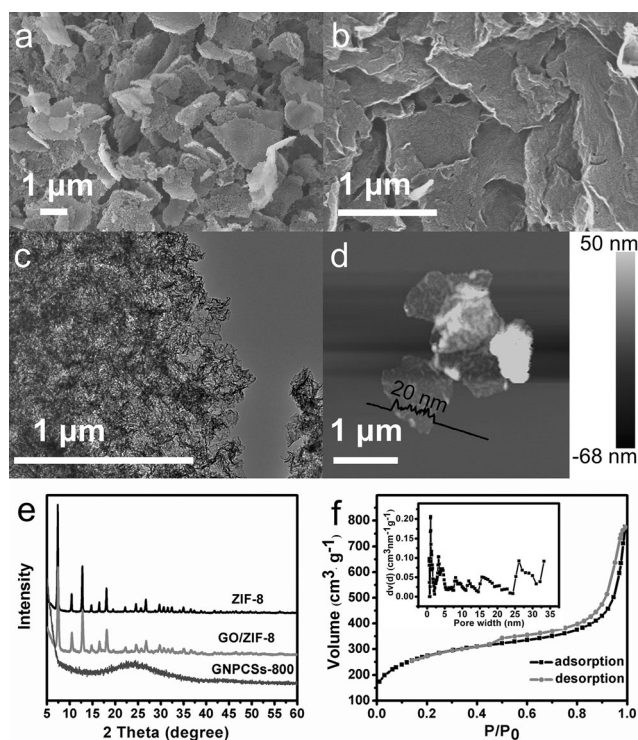


Figure 1. a) SEM image of GO/ZIF-8. SEM (b), TEM (c), and AFM (d) images of GNPCs-800. e) XRD patterns of ZIF-8, GO/ZIF-8, and GNPCs-800. f) Nitrogen adsorption–desorption isotherm of GNPCs-800 (inset: pore size distribution).

with sizes of several micrometers. The roughness of its surface, differing from that of GO (Figure S1 a), shows the successful deposition of ZIF-8 on GO surface, which is also supported by the similar XRD patterns of ZIF-8 and GO/ZIF-8 (Figure 1 e).^[17] Furthermore, the coating of ZIF-8 on GO was found to be very homogenous and complete (Figures S2 a–b and S3). FTIR spectroscopy was employed to track the growth process of GO/ZIF-8. As shown in Figure S4, the characteristic peaks of ZIF-8 emerge with increasing reaction time, while the peaks of GO and PVP gradually decrease, further confirming the complete coating of ZIF-8 on GO to form a sandwich structure. In sharp

contrast, without the help of PVP only incomplete and inhomogeneous growth of ZIF-8 on the GO surface can be obtained (Figure S6 b). The situation is similar when the ratio of zinc salt and the 2-methyl imidazole (2-MeIM) ligand is not proper (Figure S7 a,b). These results clearly demonstrate the crucial role of PVP and that an excess of the 2-MeIM ligand to zinc salt is required for the formation of uniform ZIF-8 on GO surface, highlighting the power of our strategy (Figure S8), which is shown in Scheme S2.

After the heat treatment, the GO/ZIF-8 sheets shrink and transform to GNPCs-800 (Figure 1 b), which is confirmed by the following features: the XRD pattern changes significantly with the peak at around 25° representing the interplane (002) reflection of graphite carbon.^[11a,18] The relative decrease in the D to G peak intensity before and after calcination indicates the improved graphitic degree (Figure S11).^[19] A TEM image (Figure 1 c) further confirms the sheet-like structure of GNPCs. In addition, the elemental mapping analysis (Figure S12) shows that N and C elements are homogeneously distributed, indicating that the ZIF-8 derived NPC is dispersed uniformly on graphene forming a sandwich structure, which is consistent with the existence of the residual ZIF-8 particles at two sides when the pyrolysis temperature is not high enough (Figure S2). The AFM analysis also reveals the lamellar structure of GNPCs-800 with a thickness of ca. 20 nm (Figures 1 d and S13).

The surface area and pore distribution of GNPCs-800 are analyzed by N₂ adsorption and desorption isotherms (Figure 1 f). The IV-type curves indicate the presence of mesopores and micropores, which might originate from the inheritance of porous ZIF-8 and the evaporation of NPC and graphene sheets.^[20] The BET result shows that GNPCs-800 (911 m² g⁻¹) has the highest surface area compared with NG (14.6 m² g⁻¹), NPC (519 m² g⁻¹), GNPCs-650 (516 m² g⁻¹), and GNPCs-950 (755 m² g⁻¹; Figures 1 f and S16). To understand why the surface area varies with pyrolysis temperatures, a thermogravimetric analysis was performed. As shown in Figure S17, the organic linkers of ZIF-8 start to decompose at 650 °C and the resulting Zn species may block the pore to lower the surface area. In contrast, the surface area decreases when the temperature increases to 950 °C, which might be due to the increased graphitic and stacking degree. The above results imply that GNPCs-800 would harvest superior performance toward ORR because of the existence of the abundant active sites and O₂ diffusion channels.

The ORR performance of NC highly depends on the content and type of doped nitrogen,^[8a,11a] which can be analyzed by X-ray photoelectron spectroscopy (Figure S18).^[5,7,21] The highest nitrogen content (11.3%) is observed for GNPCs-650, because of its incomplete decomposition of organic linkers (Figure 2 c). Besides, the nitrogen content of GNPCs-800 reaches 4.38% and is superior to that of its counterparts (2.95% for NG, 3.26% for NPC). For GNPCs-950, the nitrogen loss is very serious because of the instability of nitrogen at high temperature, which is consistent with previous observations.^[5,13,22] Furthermore, the N1s peaks are deconvoluted into three different types of nitrogen species: pyridinic-N (N1, 398.3 ± 0.1 eV), pyrrolic-N (N2,

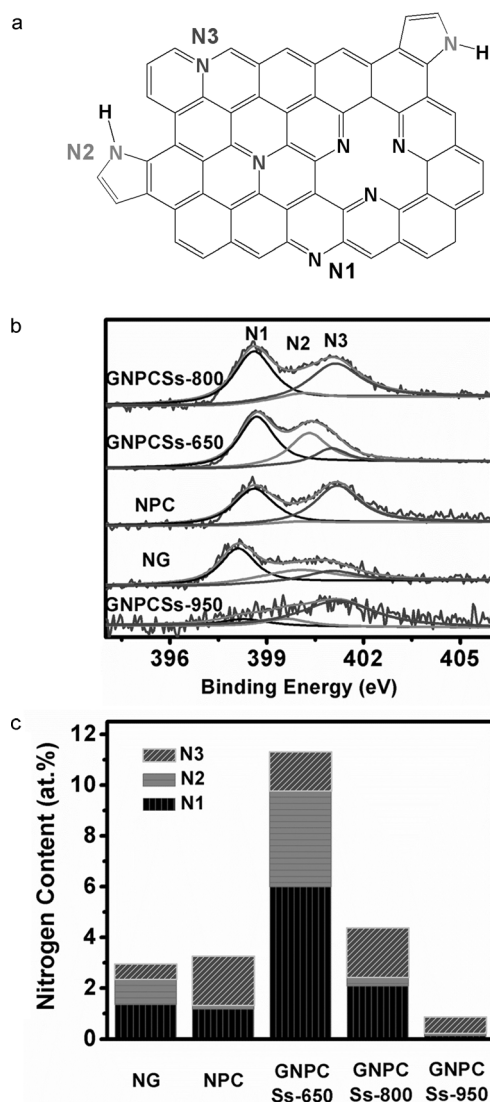


Figure 2. a) Representation of different N-based functional groups of GNPCSSs. b) High-resolution N1s spectra of NG, NPC, GNPCSSs-650, GNPCSSs-800, and GNPCSSs-950. c) The contents of N1, N2, and N3 in NG, NPC, GNPCSSs-650, GNPCSSs-800, and GNPCSSs-950.

400.0 ± 0.1 eV), and graphitic-N (N3, 401.0 ± 0.1 eV) (Figure 2a,b).^[23] In comparison, GNPCSSs-800 has higher contents of N1 and N3, which are allegedly responsible for the ORR activity.^[8a,11a,24] Besides, it is thus clear that high nitrogen content cannot assure high ORR performance.^[7,11a]

The ORR catalytic activities of the as-prepared samples are then investigated. As shown in Figure 3a, no obvious redox peak is observed for GNPCSSs-800 in Ar-saturated solution. In contrast, when the solution is saturated with O₂, a well-defined cathodic peak clearly appears at around -0.15 V, confirming the electrocatalytic activity for ORR.^[2a,25] Compared with the other samples (Figure S19), the more positive ORR peak potential of GNPCSSs-800 suggests its superior activity. The highest onset potential and largest cathodic current density are harvested by GNPCSSs-800 (Figure 3b, Tables S1, S3, and S4). Additionally, a relatively wide plateau of diffusion-limiting current is

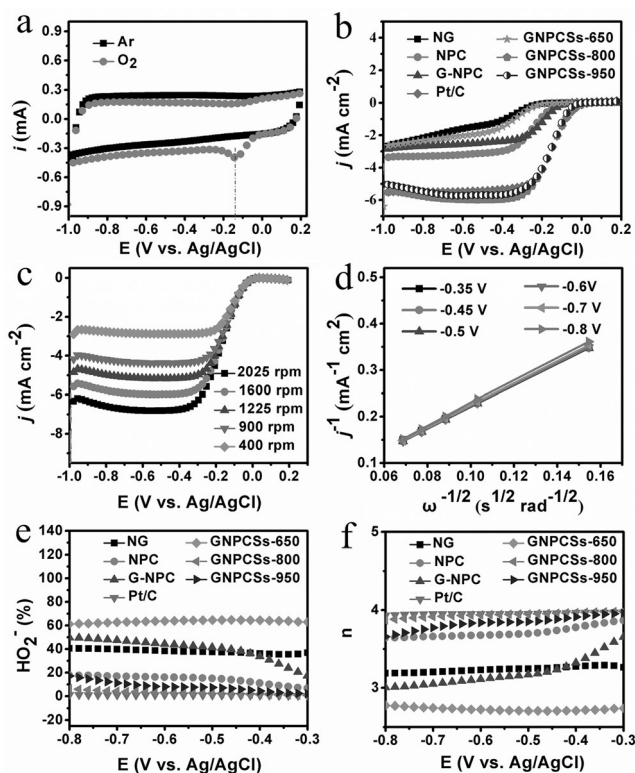


Figure 3. a) CV curves of GNPCSSs-800 in Ar-saturated and O₂-saturated 0.1 M KOH. b) ORR polarization curves for NG, NPC, G-NPC, Pt/C, GNPCSSs-650, GNPCSSs-800, and GNPCSSs-950 at 1600 rpm. c) ORR polarization curves of GNPCSSs-800 at different rotating speeds. d) K–L plots of GNPCSSs-800 at different potentials. Peroxide yields (e) and electron transfer numbers (f) of NG, NPC, G-NPC, Pt/C, GNPCSSs-650, GNPCSSs-800, and GNPCSSs-950 at various potentials based on RRDE data.

observed for GNPCSSs-800 in the polarization curve as it is also the case for Pt/C, representing the diffusion-controlled process with an efficient 4e dominated ORR pathway.^[3b,26]

Rotating disk electrode (RDE) experiments at different rotating speeds are carried out (Figure 3c) and the kinetic parameters are analyzed with the Koutecky–Levich (K–L) equation. The linearity of K–L plots for GNPCSSs-800 indicates first-order reaction kinetics with regard to the concentration of dissolved oxygen and similar electron transfer numbers (*n*) at various potentials (Figure 3d).^[3a,b] The value of *n* at -0.35 V is calculated to be 3.98, close to the theoretical value of Pt/C (4.0), indicating a near 4e ORR pathway. In contrast, *n* for NG, NPC, G-NPC, GNPCSSs-650, and GNPCSSs-950 at the same potential is only 3.1, 3.7, 3.03, 2.70, and 3.78, respectively (Figure S20), indicating the existence of a 2e reaction toward the formation of peroxide species (HO₂⁻). To quantify the ORR pathway, a rotating ring-disk electrode (RRDE) technique is conducted to monitor the formation of HO₂⁻ during the ORR process.^[3b,d] Figure 3e reveals that the measured yields of HO₂⁻ generated at the disk electrode vary over the potential range (-0.8 to -0.3 V). The HO₂⁻ yields for GNPCSSs-800 is below 10%, giving *n* of 3.78–3.98, similar to that of Pt/C, which is consistent with the results obtained from the K–L plots based on the RDE experiment. In contrast, the amounts of

HO_2^- for NG, NPC, and G-NPC are much higher, corresponding to n of 3.18–3.27, 3.63–3.82, and 2.98–3.53, respectively. For GNPCs-650, the incomplete decomposition of organic ligand affects the ORR activity severely, revealing the highest HO_2^- yields ($\approx 75\%$) and the lowest n (≈ 2.6). With respect to GNPCs-950, the great loss of ORR active N1 and N3 species at high temperature results in the relatively high HO_2^- yields ($\approx 18\%$) and low n (≈ 3.6).

To evaluate the durability of GNPCs-800 and Pt/C, chronoamperometric responses were measured.^[5,20] As displayed in Figure 4a, GNPCs-800 exhibits a slow current decrease with 94% retention over 28000 s of continuous operation, whereas Pt/C exhibits a faster current loss with

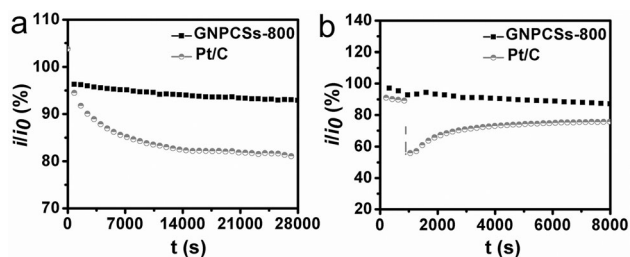


Figure 4. a) Current–time (i – t) chronoamperometric (CA) responses of GNPCs-800 and Pt/C in O_2 -saturated 0.1 M KOH at -0.4 V and 1600 rpm. b) i – t CA responses for GNPCs-800 and Pt/C at -0.4 V and 1600 rpm with 2% (v/v) methanol addition at around 900 s. i_0 defines the initial current.

only 80% retention. Subsequently, GNPCs-800 is also subjected to test the possible crossover effect caused by small organic molecules (e.g., methanol). When adding 2% (v/v) methanol, the current for GNPCs-800 is slightly changed and recovered quickly, whereas Pt/C shows a significant current decrease, suggesting GNPCs-800 shows high selectivity for ORR with strong tolerance to crossover effect and high stability.

Figure 5 shows the performance of alkaline direct methanol fuel cells (ADMFCs). The open-circuit voltage (OCV) of 0.71 V is observed for the cell with GNPCs-800 as cathode, which is slightly higher than that of 0.65 V for the cell with Pt/

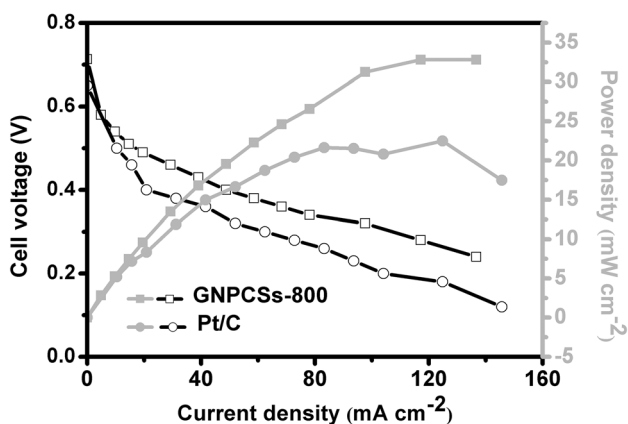


Figure 5. The cell voltage and power density of ADMFCs with GNPCs-800 and commercial Pt/C (20 wt%) as cathodes.

C and demonstrates that GNPCs-800 has a superior tolerance against methanol crossover effect in comparison with Pt/C, consistent with the above chronoamperometric results. Additionally, the corresponding peak power density of the cell with GNPCs-800 reaches 33.8 mW cm^{-2} , which is much higher than that of 22.5 mW cm^{-2} for the cell with Pt/C (Figure 5). All the above results show that GNPCs-800 can act as a promising ORR catalyst in fuel cells.

In summary, we have designed and synthesized the first ORR electrocatalyst based on graphene and ZIF-8 derived NPC through a facile, effective, and scalable approach. Unexpectedly, the resultant GNPCs-800 exhibits a high activity, good tolerance to methanol, and superior stability in comparison to commercial Pt/C catalyst, which might be attributed to the synergistic effect of graphene and NPC in terms of high electrical conductivity, high stability against corrosion during ORR, well-defined porous structures, high surface area, and favorable N composition and content. Furthermore, GNPCs-800 endows ADMFCs with much higher open-circuit voltage and power density, making it a promising ORR catalyst in fuel cells.

Received: September 11, 2014

Revised: September 24, 2014

Published online: October 21, 2014

Keywords: electrocatalysts · nitrogen doping · oxygen reduction reaction · porous carbon sheets

- [1] a) H. Wang, Y. Liang, Y. Li, H. Dai, *Angew. Chem. Int. Ed.* **2011**, *50*, 10969; *Angew. Chem.* **2011**, *123*, 11161; b) Z. Wen, S. Ci, F. Zhang, X. Feng, S. Cui, S. Mao, S. Luo, Z. He, J. Chen, *Adv. Mater.* **2012**, *24*, 1399; c) D. F. van der Vliet, C. Wang, D. Tripkovic, D. Strmcnik, X. F. Zhang, M. K. Debe, R. T. Atanasoski, N. M. Markovic, V. R. Stamenkovic, *Nat. Mater.* **2012**, *11*, 1051; d) S. Guo, S. Sun, *J. Am. Chem. Soc.* **2012**, *134*, 2492.
- [2] a) S. Chen, Z. Wei, X. Qi, L. Dong, Y. G. Guo, L. Wan, Z. Shao, L. Li, *J. Am. Chem. Soc.* **2012**, *134*, 13252; b) E. Proietti, F. Jaouen, M. Lefevre, N. Larouche, J. Tian, J. Herranz, J. P. Dodelet, *Nat. Commun.* **2011**, *2*, 416; c) S. Sun, G. Zhang, D. Geng, Y. Chen, R. Li, M. Cai, X. Sun, *Angew. Chem. Int. Ed.* **2011**, *50*, 422; *Angew. Chem.* **2011**, *123*, 442.
- [3] a) Y. Li, W. Zhou, H. Wang, L. Xie, Y. Liang, F. Wei, J. C. Idrobo, S. J. Pennycook, H. Dai, *Nat. Nanotechnol.* **2012**, *7*, 394; b) Y. Liang, Y. Li, H. Wang, J. Zhou, J. Wang, T. Regier, H. Dai, *Nat. Mater.* **2011**, *10*, 780; c) R. Bashyam, P. Zelenay, *Nature* **2006**, *443*, 63; d) Z. S. Wu, S. Yang, Y. Sun, K. Parvez, X. Feng, K. Müllen, *J. Am. Chem. Soc.* **2012**, *134*, 9082.
- [4] a) C. H. Choi, S. H. Park, S. I. Woo, *ACS Nano* **2012**, *6*, 7084; b) Z. Wang, R. Jia, J. Zheng, J. Zhao, L. Li, J. Song, Z. Zhu, *ACS Nano* **2011**, *5*, 1677; c) W. Wei, H. Liang, K. Parvez, X. Zhuang, X. Feng, K. Müllen, *Angew. Chem. Int. Ed.* **2014**, *53*, 1570; *Angew. Chem.* **2014**, *126*, 1596.
- [5] a) S. Yang, L. Zhi, K. Tang, X. Feng, J. Maier, K. Müllen, *Adv. Funct. Mater.* **2012**, *22*, 3634; b) D. S. Geng, Y. Chen, Y. G. Chen, Y. L. Li, R. Y. Li, X. L. Sun, S. Y. Ye, S. Knights, *Energy Environ. Sci.* **2011**, *4*, 760.
- [6] K. Parvez, S. Yang, Y. Hernandez, A. Winter, A. Turchanin, X. Feng, K. Müllen, *ACS Nano* **2012**, *6*, 9541.
- [7] Z. H. Sheng, L. Shao, J. J. Chen, W. J. Bao, F. B. Wang, X. H. Xia, *ACS Nano* **2011**, *5*, 4350.

- [8] a) R. Silva, D. Voiry, M. Chhowalla, T. Asefa, *J. Am. Chem. Soc.* **2013**, *135*, 7823; b) W. Ding, Z. Wei, S. Chen, X. Qi, T. Yang, J. Hu, D. Wang, L. J. Wan, S. F. Alvi, L. Li, *Angew. Chem. Int. Ed.* **2013**, *52*, 11755; *Angew. Chem.* **2013**, *125*, 11971.
- [9] H. G. Wang, Z. Wu, F. L. Meng, D. L. Ma, X. L. Huang, L. M. Wang, X. B. Zhang, *ChemSusChem* **2013**, *6*, 56.
- [10] H. W. Liang, W. Wei, Z. S. Wu, X. Feng, K. Müllen, *J. Am. Chem. Soc.* **2013**, *135*, 16002.
- [11] a) R. L. Liu, D. Q. Wu, X. L. Feng, K. Müllen, *Angew. Chem. Int. Ed.* **2010**, *49*, 2565; *Angew. Chem.* **2010**, *122*, 2619; b) J. Liang, X. Du, C. Gibson, X. W. Du, S. Z. Qiao, *Adv. Mater.* **2013**, *25*, 6226.
- [12] a) Y. Deng, Y. Cai, Z. Sun, D. Gu, J. Wei, W. Li, X. Guo, J. Yang, D. Zhao, *Adv. Funct. Mater.* **2010**, *20*, 3658; b) N. P. Stadie, J. J. Vajo, R. W. Cumberland, A. A. Wilson, C. C. Ahn, B. Fultz, *Langmuir* **2012**, *28*, 10057; c) J. Lee, J. Kim, T. Hyeon, *Adv. Mater.* **2006**, *18*, 2073.
- [13] a) S. Yang, X. Feng, X. Wang, K. Müllen, *Angew. Chem. Int. Ed.* **2011**, *50*, 5339; *Angew. Chem.* **2011**, *123*, 5451; b) J. Liang, Y. Jiao, M. Jaroniec, S. Z. Qiao, *Angew. Chem. Int. Ed.* **2012**, *51*, 11496; *Angew. Chem.* **2012**, *124*, 11664.
- [14] a) H. L. Jiang, B. Liu, Y. Q. Lan, K. Kuratani, T. Akita, H. Shioyama, F. Zong, Q. Xu, *J. Am. Chem. Soc.* **2011**, *133*, 11854; b) N. L. Torad, M. Hu, Y. Kamachi, K. Takai, M. Imura, M. Naito, Y. Yamauchi, *Chem. Commun.* **2013**, *49*, 2521.
- [15] a) S. Yang, X. Feng, L. Wang, K. Tang, J. Maier, K. Müllen, *Angew. Chem. Int. Ed.* **2010**, *49*, 4795; *Angew. Chem.* **2010**, *122*, 4905; b) L. Dai, *Acc. Chem. Res.* **2013**, *46*, 31.
- [16] a) C. Petit, T. J. Bandosz, *Adv. Mater.* **2009**, *21*, 4753; b) Z. H. Huang, G. Liu, F. Kang, *ACS Appl. Mater. Interfaces* **2012**, *4*, 4942; c) J. H. Lee, J. Jaworski, J. H. Jung, *Nanoscale* **2013**, *5*, 8533; d) M. Jahan, Z. Liu, K. P. Loh, *Adv. Funct. Mater.* **2013**, *23*, 5363; e) M. Jahan, Q. L. Bao, K. P. Loh, *J. Am. Chem. Soc.* **2012**, *134*, 6707; f) M. Jahan, Q. Bao, J. X. Yang, K. P. Loh, *J. Am. Chem. Soc.* **2010**, *132*, 14487; g) R. Kumar, K. Jayaramulu, T. K. Maji, C. N. R. Rao, *Dalton Trans.* **2014**, *43*, 7383; h) S. Liu, L. Sun, F. Xu, J. Zhang, C. Jiao, F. Li, Z. Li, S. Wang, Z. Wang, X. Jiang, H. Zhou, L. Yang, C. Schick, *Energy Environ. Sci.* **2013**, *6*, 818; i) X. Huang, B. Zheng, Z. Liu, C. Tan, J. Liu, B. Chen, H. Li, J. Chen, X. Zhang, Z. Fan, W. Zhang, Z. Guo, F. Huo, Y. Yang, L.-H. Xie, W. Huang, H. Zhang, *ACS Nano* **2014**, *8*, 8695.
- [17] a) R. Banerjee, A. Phan, B. Wang, C. Knobler, H. Furukawa, M. O'Keeffe, O. M. Yaghi, *Science* **2008**, *319*, 939; b) H. T. Kwon, H. K. Jeong, *Chem. Commun.* **2013**, *49*, 3854; c) R. Kumar, K. Jayaramulu, T. K. Maji, C. N. Rao, *Chem. Commun.* **2013**, *49*, 4947.
- [18] a) W. Yang, T. P. Fellingner, M. Antonietti, *J. Am. Chem. Soc.* **2011**, *133*, 206; b) Y. Tang, B. L. Allen, D. R. Kauffman, A. Star, *J. Am. Chem. Soc.* **2009**, *131*, 13200.
- [19] a) M. S. Dresselhaus, G. Dresselhaus, R. Saito, A. Jorio, *Phys. Rep.* **2005**, *409*, 47; b) Z. Li, Z. Xu, X. Tan, H. Wang, C. M. B. Holt, T. Stephenson, B. C. Olsen, D. Mitlin, *Energy Environ. Sci.* **2013**, *6*, 871.
- [20] W. Chaikittisilp, M. Hu, H. Wang, H. S. Huang, T. Fujita, K. C. Wu, L. C. Chen, Y. Yamauchi, K. Ariga, *Chem. Commun.* **2012**, *48*, 7259.
- [21] S. Chen, J. Bi, Y. Zhao, L. Yang, C. Zhang, Y. Ma, Q. Wu, X. Wang, Z. Hu, *Adv. Mater.* **2012**, *24*, 5593.
- [22] Y. Wang, Y. Y. Shao, D. W. Matson, J. H. Li, Y. H. Lin, *ACS Nano* **2010**, *4*, 1790.
- [23] a) P. Chen, T. Y. Xiao, Y. H. Qian, S. S. Li, S. H. Yu, *Adv. Mater.* **2013**, *25*, 3192; b) K. Ai, Y. Liu, C. Ruan, L. Lu, G. M. Lu, *Adv. Mater.* **2013**, *25*, 998; c) D. Zhao, J. L. Shui, C. Chen, X. Chen, B. M. Reprogue, D. Wang, D. J. Liu, *Chem. Sci.* **2012**, *3*, 3200.
- [24] a) Y. Y. Shao, J. H. Sui, G. P. Yin, Y. Z. Gao, *Appl. Catal. B* **2008**, *79*, 89; b) X. H. Li, M. Antonietti, *Angew. Chem. Int. Ed.* **2013**, *52*, 4572; *Angew. Chem.* **2013**, *125*, 4670.
- [25] D. S. Yang, D. Bhattacharjya, S. Inamdar, J. Park, J. S. Yu, *J. Am. Chem. Soc.* **2012**, *134*, 16127.
- [26] Y. Zheng, Y. Jiao, L. Ge, M. Jaroniec, S. Z. Qiao, *Angew. Chem. Int. Ed.* **2013**, *52*, 3110; *Angew. Chem.* **2013**, *125*, 3192.